Volume 13
Number 30
14 August 2025
Pages 24163–25152

Journal of Materials Chemistry A

Materials for energy and sustainability

rsc.li/materials-a

ISSN 2050-7488

ROYAL SOCIETY OF CHEMISTRY

PAPER

José Manuel Herrero-Martínez, Donatella Armentano, Emilio Pardo *et al.*
Efficient removal of drugs of abuse from drinking water using metal–organic frameworks

Journal of Materials Chemistry A

ROYAL SOCIETY OF CHEMISTRY

PAPER

View Article Online
View Journal | View Issue

Cite this: J. Mater. Chem. A, 2025, 13, 24473

Efficient removal of drugs of abuse from drinking water using metal–organic frameworks†

Thais Grancha, ‡[a] Patricia Garcia-Atienza, ‡[b] Sergio Armenta, [b] José Manuel Herrero-Martínez, *[b] Rita Maria Percoco, [c] Donatella Armentano, *[c] Jesús Ferrando-Soria [a] and Emilio Pardo *[a]

The presence of residues of drugs of abuse in potable water is a growing concern worldwide. Different studies have detected traces of opioids, cocaine, amphetamines, or cannabinoids in surface water, groundwater, and even treated drinking water, which is a clear indicator of insufficient removal during wastewater treatment processes. These substances may persist in the environment, posing potential long-term risks to human health and ecosystems, and consequently, making the quest for efficient decontamination technologies mandatory. Herein, we explore the use of a family of six eco-friendly water-stable isoreticular metal–organic frameworks (MOFs) and multivariate MOFs (MTV-MOFs), prepared from amino acids, as adsorbents for the removal of a mix of 29 drugs of abuse from water. Among them, the MOF prepared from the natural amino acid L-methionine, with the formula $\{Ca^{II}Cu^{II}_6[(S,S)\text{-methox}]_3(OH)_2(H_2O)\}\cdot 16H_2O$ (**3**), features channels densely decorated with thioalkyl ($-CH_2CH_2SCH_3$) residues and exhibits an outstanding removal efficiency being capable to remove them almost completely in a single capture step under dynamic solid-phase extraction conditions (less than 30 seconds). Also, the removal performance of **3** toward the highly concerning drug fentanyl –responsible for a large number of deaths due to overdose in the United States and Canada was further investigated. **3** is capable of capturing fentanyl entirely, for at least 16 consecutive cycles, outperforming the current reference material, powdered activated carbon (PAC). Finally, the crystal structures of two host–guest adsorbates with amphetamine molecules embedded within the channels of two of the MOFs of the family $\{Sr^{II}Cu^{II}_6[(S,S)\text{-mecysmox}]_3(OH)_2(H_2O)\}\cdot 15H_2O$ (**2′**) and (**3**) could be resolved, helping to unveil the interactions between the drugs and the MOF matrix. Moreover, the crystal structure of another host–guest adsorbate with fentanyl molecules hosted in MOF $Sr^{II}Cu^{II}_6[(S,S)\text{-methox}]_3(OH)_2(H_2O)\}\cdot 16H_2O$ (**3′**) was also elucidated. Overall, these properties situate MOF **3** among the most attractive adsorbents for the challenging removal of such emerging pollutants and it is a viable alternative for application in a real-world environment.

Received 24th February 2025
Accepted 15th May 2025

DOI: 10.1039/d5ta01530h

rsc.li/materials-a

1. Introduction

Contamination of waste and surface waters by a wide diversity of emerging pollutants constitutes one of the biggest concerns for modern societies.[1] In particular, the presence in aquatic environments of drugs of abuse[2–7] – a term that includes both prescription and illicit drugs – and their metabolites, attracts increasing scientific interest, given their potential adverse impact on aquatic organisms[8] and, ultimately, on human health.[9] As a representative example, in recent years, a tremendous social crisis has unfolded in the United States and Canada due to the abusive consumption of fentanyl,[10,11] which is a synthetic opioid medication approved by the Food and Drug Administration for use as an analgesic and anaesthetic. After being consumed, fentanyl, as well as other drugs of abuse, are excreted to wastewaters and finally reach treatment plants. However, current purification technologies used in sewage treatment plants – *i.e.* chemical, photochemical or biological degradation of organic pollutants and/or their adsorption by traditional porous materials – present certain limitations, not achieving their complete removal, and consequently, many of them have been detected in drinking waters in North America and Europe.[7,9,12,13] This is particularly concerning, taking into account that wastewater reuse has become more common in

[a]Instituto de Ciencia Molecular (ICMol), Universidad de Valencia, 46980 Paterna, Valencia, Spain. E-mail: emilio.pardo@uv.es

[b]Departamento de Química Analítica, Universitat de València, c/Dr Moliner, 50, 46100 Burjassot, Valencia, Spain. E-mail: jmherrer@uv.es

[c]Dipartimento di Chimica e Tecnologie Chimiche (CTC), Università della Calabria, Rende 87036, Cosenza, Italy. E-mail: Donatella.armentano@unical.it

† Electronic supplementary information (ESI) available: CCDC 2415524–2415526. For ESI and crystallographic data in CIF or other electronic format see DOI: https://doi.org/10.1039/d5ta01530h

‡ These authors have contributed equally to this work.

recent years, and it will keep increasing, due to the global water crisis, which increases the risk of these drugs being ingested by humans if purification is inadequate.[14] Thus, new technologies are needed to make front to the pressing need of efficiently removing these emerging pollutants.

Current technologies operating in sewage treatment plants for general organic pollutants include chemical, photochemical or biological degradation and/or their adsorption by traditional porous materials.[12] However, existing technologies, as mentioned above, exhibit certain limitations regarding the removal of emerging organic contaminants, such as drugs of abuse. Thus, new technologies are required to be developed to make front to the pressing need that represents the efficient capture of these emerging pollutants. Among the different possibilities, *a priori*, a capture technology-approach of the pollutant[15–17] seems particularly appealing compared to a degradation one, which may lead to the formation of other dangerous intermediate species. Therefore, the development of novel porous materials with improved affinity for drugs of abuse represents both a strong approach and a necessity. Metal–organic frameworks[18–21] (MOFs) have gained relevance in recent decades and represent a very special class of porous materials given their unique characteristics, such as large surface areas, tunable pore size, an outstanding host–guest chemistry[19] and the possibility to finely functionalize, pre- or post-synthetically,[22] their channels. As a result, MOFs find application in many different important fields, including water remediation.[23–27] Indeed, a good number of studies have been published reporting good performances for capturing inorganic[28] (*i.e.* heavy metals) and several organic contaminants, such as dyes,[29] insecticides[30] and antibiotics.[31] Moreover, in contrast to other porous materials, MOFs offer the possibility to use single crystal X-ray diffraction[32–35] (SCXRD) as a basic characterization tool. This allows us to gain insight into the crystal structure of the host–guest aggregate, that is the MOF containing the captured contaminant inside its channels, which helps to unveil the nature of the host–guest interactions governing the capture process.

However, despite all these remarkable advances, the use of MOFs for the removal – or detoxification – of drugs of abuse has not been fully exploited so far, and just few examples have been reported to date.[36,37] In this context, taking advantage of the excellent previous results of a family of water and pH resistant[38] amino acid oxamidato-based MOFs (Scheme 1) in the capture of other emerging inorganic[39–42] and organic pollutants,[29–31,43–46] we explore herein the performance of six members of this family toward the capture of drugs of abuse. In particular, we have explored the efficiency of three previously reported MOFs, with formulae $\{Ca^{II}Cu^{II}_6[(S,S)\text{-serimox}]_3(OH)_2(H_2O)\}\cdot 39H_2O$[46] (**1**), $\{Ca^{II}Cu^{II}_6[(S,S)\text{-mecysmox}]_3(OH)_2(H_2O)\}\cdot 16H_2O$[40] (**2**) and $\{Ca^{II}Cu^{II}_6[(S,S)\text{-methox}]_3(OH)_2(H_2O)\}\cdot 16H_2O$[42,47] (**3**) (where serimox = bis[(*S*)-serine]oxalyl diamide; mecysmox = bis[*S*-methylcysteine]oxalyl diamide and methox = bis[(*S*)-methionine]oxalyl diamide). Moreover, we have also used three mixed-ligand or multivariate MOFs[44,48,49] (MTV-MOFs) – possessing multiple organic linkers with different functional groups coexisting within the same framework topology[50] – with the same purpose.

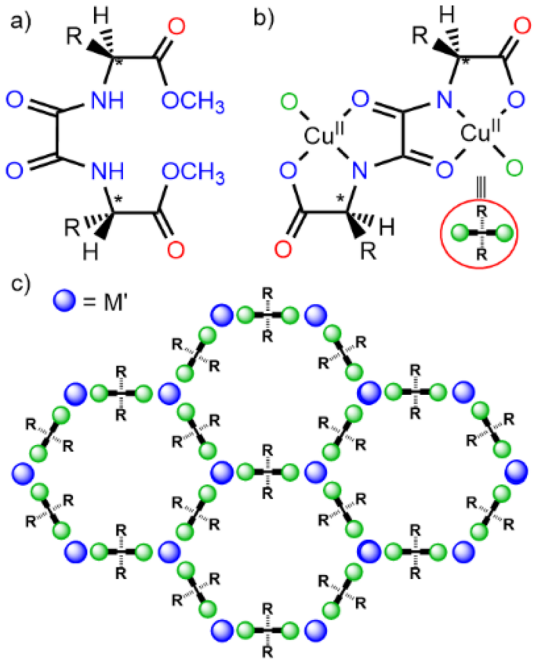

Scheme 1 Chemical structures of the amino acid-based oxamidato ligands (a) and dicopper(II) precursor complexes (b), as well as a schematic representation of the MOF hexagonal network emphasizing the position of the amino acid residues (R = $-CH_2OH$ (100%) MOF **1**; $R = -CH_2SCH_3$ (100%) MOF **2**; $R = -CH_2CH_2SCH_3$ (100%) MOF **3**; R = $-CH_2OH$ (50%) and $-CH_2CH_2SCH_3$ (50%) MOF **4**; R = $-CH_2SCH_3$ (50%) and $-CH_2CH_2SCH_3$ (50%) MOF **5**; R = $-CH_2OH$ (66.6%) and $-CH_2(C_3H_3N_2)$ (33.4%) MOF **6**).

Specifically, we have used three previously reported MTV-MOFs with formulae $\{Ca^{II}Cu^{II}_6[(S,S)\text{-methox}]_{1.5}[(S,S)\text{-serimox}]_{1.50}(OH)_2(H_2O)\}\cdot 30H_2O$[44] (**4**), $\{Sr^{II}Cu^{II}_6[(S,S)\text{-methox}]_{1.5}[(S,S)\text{-mecysmox}]_{1.50}(OH)_2(H_2O)\}\cdot 36H_2O$[30,39] (**5**) and $\{Ca^{II}Cu^{II}_6[(S,S)\text{-serimox}]_2[(S,S)\text{-hismox}]_1(OH)_2(H_2O)\}\cdot 27H_2O$[51] (**6**) (where hismox = bis[(*S*)-histidine]oxalyl diamide) (Scheme 1 and Fig. 1).

2. Results and discussion

In this work, we first explored the efficiency of MOFs **1–3** and MTV-MOFs **4–6** towards the capture of drugs of abuse. For this purpose, we evaluated their efficiency, as sorbents for solid-phase extraction (SPE), towards a mixture containing 29 drugs of abuse (Schemes S1–S3† and Table 1). Overall, they exhibited very good capture properties and they were capable to remove them, very efficiently, in a single loading step, within 30 seconds. Remarkably, MTV-MOF **5** and, especially, MOF **3** – featuring functional pores decorated with $-CH_2CH_2SCH_3$ and $-CH_2SCH_3$ (1 : 1) in the case of **5** and highly flexible $-CH_2CH_2SCH_3$ residues in the case of **3** – exhibited outstanding performances, being capable to capture most of them (>90%) in a single capture process. On this basis, we then selected MOF **3**, which demonstrates the highest efficiency, and studied its reusability against an emerging contaminant of great current relevance, fentanyl. Indeed, it was observed that MOF **3** is capable of capturing fentanyl up to 16 consecutive times with

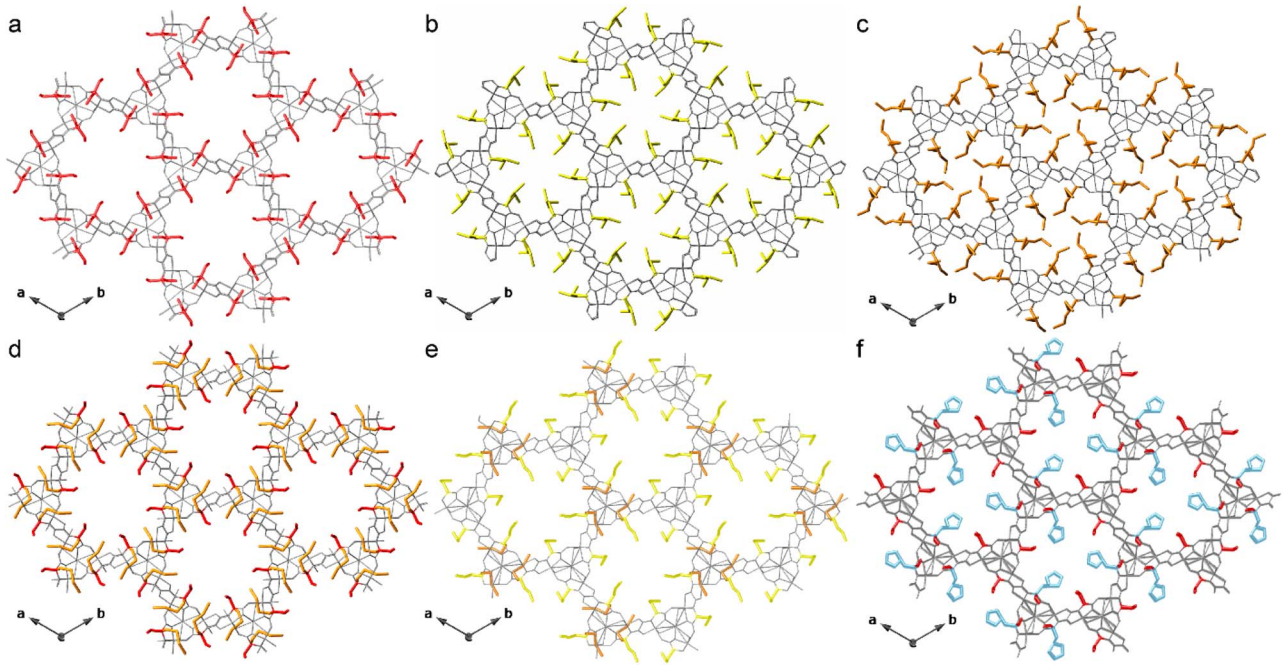

Fig. 1 Perspective views of the crystal structures of MOFs **1** (a), **2** (b), and **3** (c) and MTV-MOFs **4** (d), **5** (e) and **6** (f). Metal atoms and organic ligands are represented as thin grey sticks with the exception of amino acid residues, which are depicted as red ($-CH_2OH$ from L-serine), yellow ($-CH_2SCH_3$ from *S*-methyl-L-cysteine), orange ($-CH_2CH_2SCH_3$ from L-methionine) and blue thick sticks ($-CH_2C_3H_3N_2$ from L-histidine) to emphasize the functionalization of the channels.

percentages very close to 100%. Finally, the high crystallinity of this family of MOFs allowed us to resolve the crystal structures (Table S1†) of different host–guest adsorbates with amphetamine or fentanyl molecules embedded within the channels of some of these MOFs (*vide infra*). These structures allow for the visualization and analysis of the host–guest interactions present in all cases, establishing a relationship between these interactions and the capture properties in these MOFs.

2.1 Crystal structures of MOFs 1–6

Fig. 1 shows the crystal structures of **1–6**. These materials are isoreticular crystalline structures that crystallize in the chiral $P6_3$ space group of the hexagonal system. Their architecture consists of acs chiral, honeycomb-like 3D networks formed by calcium(II) or strontium(II) ions coordinated with copper(II) centres, creating hexagonal channels with pore sizes ranging from approximately 0.3 nm to 0.8 nm. Within these pores, adaptable amino acid residues are confined (refer to colour coding in Fig. 1). This confinement imparts exceptional intrinsic flexibility to the pores, enabling the frameworks to adjust their conformation based on the size, shape, and chemical properties of guest molecules. Furthermore, the inclusion of diverse amino acid-derived moieties within the same confined space – MTV-MOFs – introduces additional functional diversity (Fig. 1d–f). This adaptability, combined with a robust and resilient backbone, allows oxamidato-based MOFs to endure harsh environmental conditions while maintaining the versatility necessary for selective interactions with a wide range of guest molecules.

2.2 Capture experiments

Prior to exploring the capture capacities of **1–6**, their permanent porosity was evaluated by measuring their N_2 adsorption isotherms on fresh polycrystalline samples, which are identical to those previously reported (Fig. S1†). In particular, they exhibit Brunauer–Emmett–Teller[52] (BET) surface areas of 860.7 (**1**), 716.2 (**2**), 177.7 (**3**), 657.7 (**4**), 570.8 (**5**) and 258.7 (**6**) $m^2\ g^{-1}$ with calculated pore sizes[53] of 0.88 (**1**), 0.78 (**2**), 0.20 (**3**), 0.71 (**4**), 0.62 (**5**) and 0.28 (**6**) nm (Fig. S2†), which approximately correspond to those determined from the crystal structures. The shape and size of these polycrystalline powders can be observed by taking MOF **3** as a representative example and capturing images of this sample using scanning (SEM) and transmission electron microscopies (TEM) (Fig. 2 and S3,† respectively), which also permitted us to obtain the corresponding elemental mapping that shows a homogeneous distribution of Cu, Ca and S in the sample (Fig. S4†).

Once the porous nature of **1–6** was confirmed, aiming at evaluating the capture properties of the family, SPE devices were prepared by packing 25 mg of the corresponding polycrystalline samples – with particle sizes ranging approximately from 1 to 6 μm (Fig. 2) – of MOF/MTV-MOFs (**1–6**) between two frits into 1 mL empty propylene cartridges (Fig. S5†). To avoid sorbent losses, before introducing the MOF into the cartridge, a nylon filter was cut and placed on the top of the bottom frit. Initially, the adsorbent underwent activation and equilibration using 2 mL of CH_3OH followed by 2 mL of H_2O. Then, a 1 mL aqueous mixture containing 29 drugs of abuse, each at a concentration of 20 μg L^{-1}, was percolated through the SPE cartridges. A

Table 1 Removal values (%) for drugs of abuse from an aqueous solution containing a mixture of 29 different drugs (20 μg L^{-1} for each pollutant) using MOFs **1–6**

	Removal efficiency (%)					
Drug	**1**	**2**	**3**	**4**	**5**	**6**
Fentanyl	**100.0**	**100.0**	**99.0**	**99.9**	**100.0**	74.8
Nicotine	75.0	66.3	**94.4**	82.1	80.1	30.9
LSD[a]	78.3	69.5	**100.0**	70.5	68.1	41.5
Ketamine	43.4	33.5	**96.3**	53.1	55.9	19.0
Amphetamine	54.1	87.6	**100.0**	82.2	**93.4**	46.0
Methamphetamine	47.3	39.3	**100.0**	73.9	85.4	28.5
Benzoylecgonine	19.3	7.0	23.0	0.0	5.4	0.0
Cocaine	78.1	82.9	**99.6**	**93.7**	**96.6**	77.1
3MeO-PCP[b]	**100.0**	**100.0**	**100.0**	**100.0**	**100.0**	78.2
Butylone	35.2	56.8	**98.7**	77.2	86.0	24.0
Cathinone	81.8	18.7	**100.0**	82.9	57.2	72.4
Metilone	27.6	**100.0**	**98.6**	**100.0**	88.8	21.1
Heroin	86.1	75.8	**100.0**	85.3	76.6	74.4
MDMA[c]	44.6	47.7	**99.7**	79.4	**91.7**	26.0
α-PVP[d]	63.0	73.7	**100.0**	82.8	**90.7**	53.3
Caffeine	37.3	20.0	52.2	9.9	19.7	34.4
Diazepam	88.3	85.6	**100.0**	**91.4**	**90.5**	55.8
Codeine	0.0	6.3	71.3	0.0	0.0	0.0
Oxazepam	83.7	87.4	**100.0**	87.9	**94.6**	64.5
Norketamine	57.4	69.6	**100.0**	89.3	**93.3**	26.2
EME[e]	88.3	**90.2**	**99.9**	**92.5**	**94.9**	**92.5**
6-MAM[f]	22.5	0.0	**91.3**	34.8	21.0	0.0
Alprazolam	**97.9**	**98.0**	**100.0**	**98.5**	**99.4**	72.8
Methadone	**100.0**	**100.0**	**100.0**	**100.0**	**100.0**	**99.4**
Buprenorphine	**100.0**	**100.0**	**100.0**	**100.0**	**100.0**	**100.0**
Tramadol	52.0	48.8	**100.0**	77.5	82.3	16.8
Chlordiazepoxide	61.0	52.1	**92.9**	56.8	58.4	40.8
Naphazoline	88.8	**98.1**	**100.0**	**97.5**	**99.6**	84.7
Clorazepate	84.2	89.5	**100.0**	**94.2**	**96.6**	67.6

[a] LSD = lysergic acid diethylamide. [b] 3MeO-PCP = 3-methoxyphencyclidine. [c] MDMA = 3,4-methylenedioxymethamphetamine. [d] α-PVP = alpha-pyrrolidinovalerophenone. [e] EME = Ecgonine methyl ester. [f] 6-MAM = 6-monoacetylmorphine. Removal efficiencies higher than 90% are represented in bold to highlight the goodness of each material.

washing step with 1 mL of H_2O was then conducted. In order to properly quantify the retained drugs of abuse within MOF channels, a solution of CH_3OH (5 mL) was passed through the SPE cartridge to extract them. All SPE fractions were collected and filtered through a membrane with a pore size of 0.22 μm, and subsequently injected into a HPLC-MS system to determine the removal percentage. All the presented capture experiments were conducted in triplicate (additional details can be found in the ESI†). The breakthrough volume of the developed MOF cartridges has been evaluated using the multicomponent drug solution at a 20 μg L^{-1} concentration level and a 20 mg sorbent bed, obtaining a minimum value of 50 mL without appreciable analyte losses. Here, we would like to remark that the complexity of the proposed experiment goes beyond the common kinetic study under dispersive conditions – where the extraction is governed by equilibrium kinetics.[17] Such studies, apart from providing researchers with information of the adsorption mechanism of individual guests, represent an indirect manner to test the goodness of a selected adsorbent for real world applications. We consider that if a selected material is able to capture efficiently in such a complex matrix and in a continuous mode (*i. e.* less than 30 s of contact time between the percolated solution and MOF), it is clear and direct evidence of their goodness as adsorbents for drugs of abuse. For this reason, eager to take MOFs for water remediation to the next level, we have centred the study on the efficient removal performance of selected MOFs toward a mix of 29 drugs of abuse under continuous cartridge SPE conditions – a non-equilibrium, exhaustive extraction procedure based on multi-step equilibrium of analytes between the SPE column plates and MOFs.

The results are shown in Table 1 (see also Table S2†). Notably, even if the six MOFs were capable of adsorbing the drugs, they exhibited quite distinct behaviours. MTV-MOF **6** – possessing 50% of $-CH_2C_3H_3N_2$ and 50% of $-CH_2OH$ groups decorating the channels – shows, by far, the worst capture properties of the whole family. In turn, the capture properties of MOF **1**, – possessing only $-CH_2OH$ groups from L-serine amino

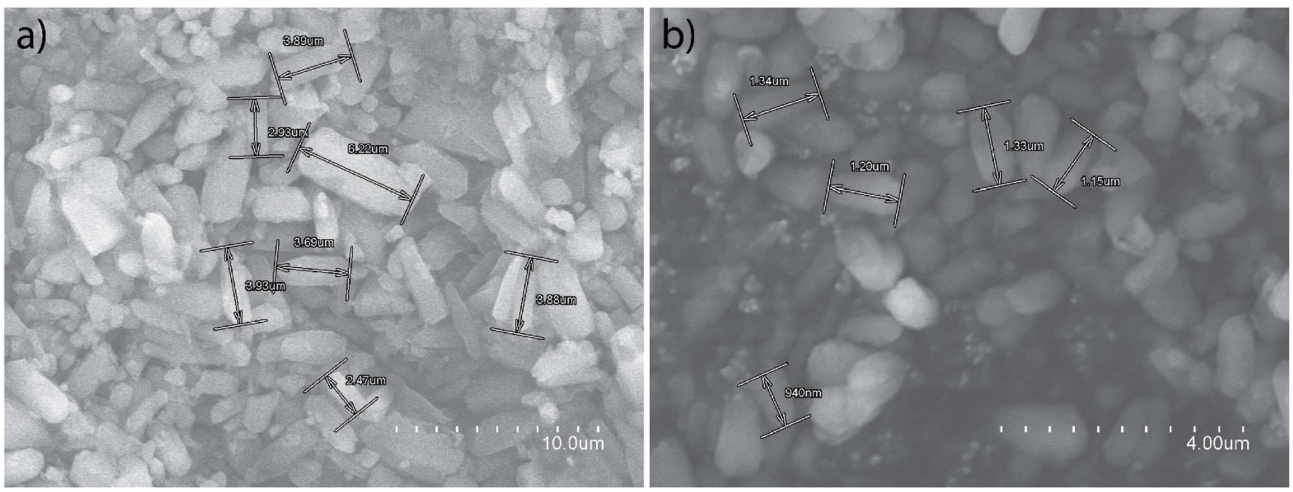

Fig. 2 SEM images of a polycrystalline sample of **3** at two different magnifications (a and b) with selected sizes marked.

acids – are somewhat improved suggesting that imidazole residues are not efficient in the removal of drugs of abuse. On the other hand, for MOFs containing sulphur-derived arms, that is MOFs **2–5**, derived from L-methionine and *S*-methyl-L-cysteine amino acids, capture properties are enormously improved (Table 1). In particular, the L-methionine derived MOF (**3**) shows impressive capture properties and is capable to adsorb the vast majority of them in percentages close to 100% (Table 1). Extracted chromatograms for each analyte, before and after capture experiments with MOF **3**, can be seen in Fig. S6.† Based on previous results with MOF **3**,[29–31,42,47] two main reasons arise to explain such outstanding capture properties. First, thioether groups located in the channels have already shown great capacities to establish weak intermolecular interactions, including the frequently underestimated σ–hole interactions,[29] with host organic molecules. Secondly, $-CH_2CH_2SCH_3$ "arms" exhibit great flexibility/adaptability,[54] and they are capable to adjust in order to accommodate guest molecules by maximizing the host–guest interactions mentioned above. MOF **3** exhibits a very remarkable adsorption for almost all the drugs of abuse presented in this work, as well as for other emerging contaminants, such as antibiotics, insecticides and organic dyes, previously reported.[29–31] Here, we would like to emphasize that this is a very strong feature of the adsorbent, especially when considering real-world applications in wastewater treatment plants. The goal is to develop an adsorbent capable of efficiently removing as many different emerging organic contaminants as possible at once—something that current technologies do not adequately address.

In order to rationalize the observed experimental results, we have represented the removal efficiency for each studied MOF in front of an intrinsic physical property of the analytes, such as Log *P* – the octanol–water partition coefficient, which measures the hydrophobicity of the target analytes – and pK_a (Fig. S7 and S8†). Log *P* ranged from −1.3 for benzoylecgonine to 4.98 for buprenorphine. The broad range of this physical property, coupled with the wide range of pK_a values the investigated drugs of abuse exhibit, poses a significant challenge for their simultaneous extraction and analysis, which reinforces the goodness of MOF **3** as an adsorbent.[55] Fig. S7 and S8† show the correlation between the extraction efficiency of the different evaluated MOFs and Log *P* and pK_a values of the analytes. In general, a positive correlation can be observed between the extraction efficiency and the Log *P* value of the analytes. When log *P* increases, the extraction efficiency tends to increase across all the evaluated MOFs. This may explain the lower removal efficiency for benzoylecgonine and caffeine, as they present negative log *P* values, indicating that both possess strong hydrophilic character with a greater affinity for water. For pK_a it is hard to find any correlation. This can most likely be attributed to the fact that the adsorption process is influenced by the simultaneous action of several factors to different extents.

Under the premise of these spectacular results, we then decided to establish the reusability of MOF **3**. For this, we selected a particular drug of abuse, fentanyl, due to its great current social importance,[11] and we carried out a study of capturing this drug in 16 consecutive cycles. In order to do so, we have passed through the SPE cartridges 1 mL of 20 μg L^{-1} fentanyl aqueous solution and analysed the eluents after each cycle, as previously described for the mix capture experiment. Noteworthily, to explore the potential application of **3** in a real-world setting, where it is impractical to regenerate the material after each decontamination process, we have performed the cycles without regenerating the material, with only a small volume of eluent (2 mL) passed between measurements to remove residual absorbed analytes at MOF particle surfaces. For each of these 16 experiments, virtually 100% capture was observed in all cases (Fig. 3 and Table S2†), suggesting a significant applicability of this material under real conditions. In addition, in order to compare this compound with the reference material commonly used in decontamination, the well-known powdered activated carbon (PAC), we repeated the same 16 capture experiments for this material. Indeed, PAC also exhibited outstanding capture properties –comparable to those of MOF **3** – for the first 10 capture cycles. Remarkably, from 11th reuse, **3** starts to improve PAC efficiency. Thus, after 16 reuses, our material surpasses PAC by 5%, as it is only capable of capturing 95% of the fentanyl present in the solution (Fig. 3).

2.3 Crystal structures of host–guest adsorbates

All these capture experiments demonstrate that the entire family of MOFs shows more than satisfactory capture results, being particularly remarkable for **3**. In this context, and with the aim of elucidating the host–guest interactions that account for this capture efficiency, the next step was to attempt to resolve the crystalline structures of two different host–guest aggregates, with amphetamine molecules embedded within the channels of thioether-decorated MOFs **2** and **3**. Thus, insertion experiments were carried out on single crystals of **3** and also crystals of **2′** (with the formula $\{Sr^{II}Cu^{II}_6[(S,S)\text{-mecysmox}]_3(OH)_2(H_2O)\}\cdot 15H_2O$[56] (**2′**)), which is an isoreticular MOF to **2**, where Ca^{II} cations are replaced by Sr^{II} and the resulting crystals better resisted the single-crystal to single-crystal process[22] than **2** (see

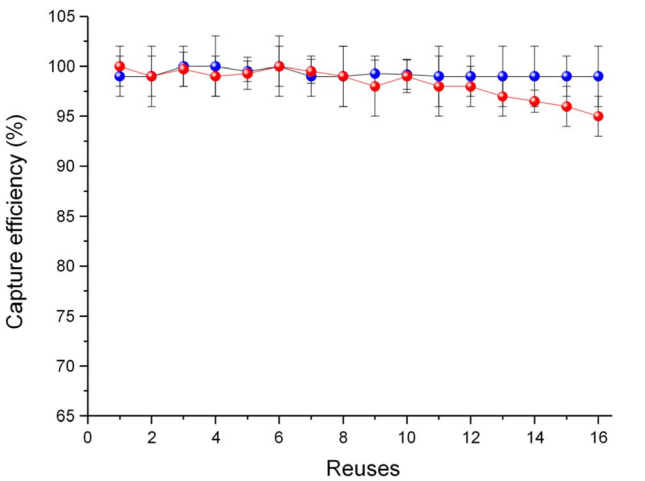

Fig. 3 Reuses of MOF **3** (blue) and activated carbon (red) for the removal (%) of fentanyl using a 20 μg L^{-1} aqueous solution. Error bars of three independent replicate measurements are included.

ESI†, experimental section). Thus, samples of host–guest aggregates of **2′** and **3** with amphetamine –suitable for single-crystal X-ray diffraction (SCXRD) and named **amphetamine@2′** and **amphetamine@3** – were obtained, and their crystal structures could be determined (Table S1†). In this sense, the N_2 adsorption isotherms of **amphetamine@2′** and **amphetamine@3** were measured (Fig. S9†) and show a decrease of *ca.* 43 and 51% compared to those of **2** and **3**, respectively, which must be attributed to the partial occupation of the pores of both MOFs with amphetamine molecules in **amphetamine@2′** and **amphetamine@3**.

Although amphetamine molecules were disordered in the pores, we succeeded in getting their possible configurations and locations (see the ESI† for structural details), as well as details on their main interaction sites with the hosting matrices **2′** and **3** (Fig. 4, 5 and S10–S12†). Compounds **amphetamine@2′** and **amphetamine@3** are isomorphs to **2**, **2′** and **3**, respectively and crystallize in the $P6_3$ chiral space group of the hexagonal system, confirming the preservation of the 3D network of the hosting matrices **2′** and **3** even after guest capture. The crystal structures clearly show that amphetamine guest molecules are encapsulated in the nanopores of **2′** and **3**, where they are simultaneously recognized by the methyl-cysteine and methionine residues, respectively. In the **amphetamine@2′** crystal structure, the most stabilizing forces are assured by strong S/π interactions,[57] (known also as π-hole interactions) where sulfur atoms interact with the amphetamine phenyl ring (APh) [S⋯$APh_{centroid}$ and S⋯$APh_{mean\ plane}$ of 3.55 and 2.40 Å, respectively] (Fig. 5a). On the other hand, in the **amphetamine@3** crystal structure, the prominent host–guest interaction is of the type σ-hole, which are available for interaction with electron donors such as nitrogen atoms exhibiting a $S_{mecys}\cdots N_{amphetamine}$ distance of 3.8 Å, shorter than the sum of van der Waals radii (Fig. 5b). Hence, despite the identical nature of guest molecules, methyl-cysteine and methionine arm conformations make the difference. The longer thioether chains in **3**, distend their conformation and move the guest towards the centre of the channels with amphetamine molecules orienting in such a way to confine the aromatic side towards the hidden centre of the pores (Fig. 4b, 5, S11 and S13b†). In contrast, the shorter methyl-cysteine arms leave enough space for the larger amphetamine aromatic rings located in the nest formed near the walls of the hosting matrix **2′** (Fig. 4a, 5b, S10 and S12a†). In doing so, in both **2′** and **3** only one of the two crystallographically distinct methyl-cysteine (**2′**) and methionine (**3**) moieties show a distended conformation, confining the other one in the small voids, generated along the *a* crystallographic axis, in a more bent conformation (Fig. 5a).

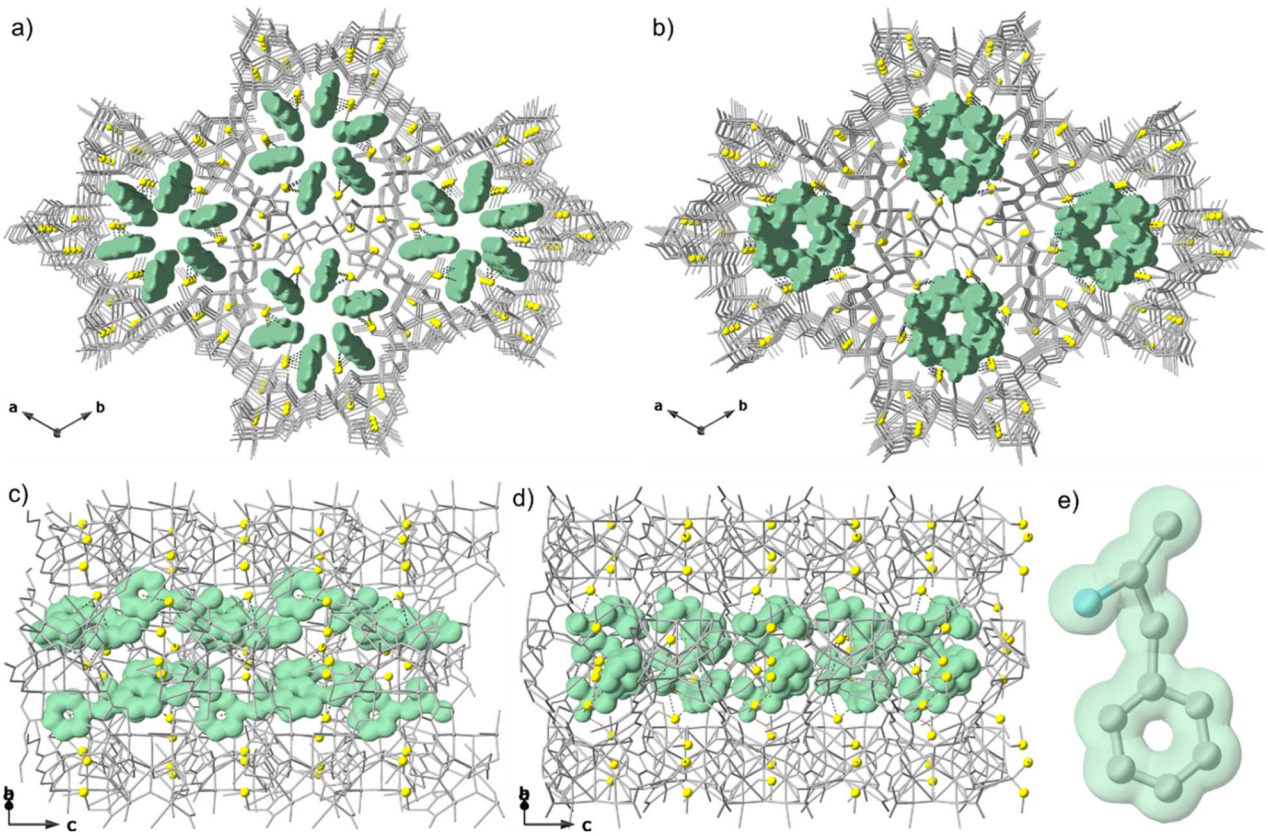

Fig. 4 Crystal structures of the host–guest aggregates **amphetamine@2′** (a) and **amphetamine@3** (b) along the *c* axis. View of a single channel of **amphetamine@2′** (c) and **amphetamine@3** (d) along the *b* axis. (e) Structure of the amphetamine molecule. Metals and organic ligands, with the exception of sulphur atoms, constituting the network are represented with grey sticks. Green surfaces are used to emphasize the guest amphetamine molecules. Colour code: grey: carbon atoms; blue: nitrogen atoms.

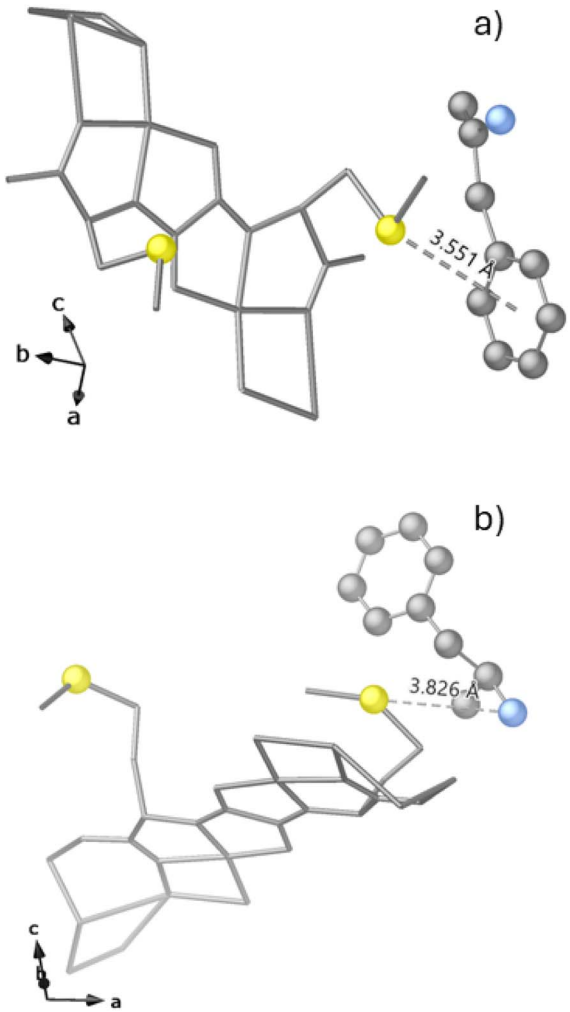

Fig. 5 Details of the crystal structure of **amphetamine@2′** (a) and **amphetamine@3** (b) showing the most stabilizing forces for the host–guest aggregates. Metal ions and organic ligands, except for sulfur atoms (yellow spheres) and guest amphetamine molecules are represented with gray sticks. Color code: gray: carbon atoms; light blue: nitrogen atoms.

The slightly higher performance of **3** *versus* **2′** for amphetamine capture could be hypothesized with the help of X-ray crystallography. Interactions found in **amphetamine@2′** and **amphetamine@3** have been discussed both in the context of sulphur-base interactions, involving low-lying sulphur σ* orbitals (known as σ-hole or π-hole in **amphetamine@2′** and **amphetamine@3**, respectively). σ- and π-holes are a particular class of less explored non-covalent interactions, whose relevance has been underestimated despite their relevance in nature, and they have been identified as key agents in the molecular recognition and capture of emergent contaminants in our family of MOFs.[29–31] Even though the strength of these interactions can largely vary depending on the specific molecular context, their overall energy of interactions for similar distances to the ones observed in the obtained host–guest aggregates was found to lie in the range of 20–40 kcal mol^{-1}. Thus, they are relatively weak and reversible, which is advantageous for recycling purposes. Lower interaction energies facilitate the release of captured guests under mild conditions, such as washing with a polar solvent, thereby enhancing the material's recyclability. However, when facing such dangerous contaminants, we consider it worth mentioning that the use of biocompatible MOFs that allow the safe disposal of the drugs of abuse-loaded material represent a safer and preferred option compared to desorption/recycling of the MOF adsorbent, thus mitigating any potential risks associated with residual contamination. In this scenario, in terms of energy involved for host–guest stabilizing effects **2′** and **3** might be considered very similar. However, the differentiation point is related to the static and dynamic features of each pore, and the higher size of the residue and flexibility of **3** *versus* **2′**, which ensures the most efficient close packing observed, could definitively be at the origin of the better performance in capture of drugs.

Finally, aiming at completing this work by elucidating the interactions enabling such extraordinary capture of fentanyl – a molecule of significant current interest – we also attempted to resolve the structure of a new host–guest adsorbate by encapsulating this molecule (fentanyl) in the most efficient MOF (**3**). For that, as previously done with MOF **2** and amphetamine molecules, we used crystals of **3′** (an isoreticular $SrCu_6$ analogue to **3** with the formula $\{Sr^{II}Cu^{II}_6[(S,S)\text{-methox}]_3(OH)_2(H_2O)\}\cdot 16H_2O$[29]), which better resisted fentanyl insertion, retaining crystallinity after insertion (see ESI,† experimental section). Thus, after completing the insertion process of these molecules within the MOF by immersing crystals of MOF **3′** in a saturated aqueous fentanyl solution for one week, a new adsorbate structure, named **fentanyl′@3′** was obtained. However, this structure shows only a fragment of the fentanyl molecule (termed fentanyl′) within the MOF pores, suggesting that the molecule undergoes fragmentation, as previously reported.[58] This could be due to the combination of two propitious factors that trigger the known fragmentation: (i) the conditions required to carry out the insertion of the target molecules into the MOF involve prolonged exposure of a concentrated aqueous solution of the guest molecules (amphetamine or fentanyl) in the presence of the corresponding oxamidato-based MOF, which is known to provide a basic medium,[38] and (ii) the oxamidato-based MOF can catalyse the degradation of this molecule upon long exposure as also observed before.[59,60] This may well explain the degradation phenomenon.[58] Please note the different time-scale for the capture experiments with respect to the crystallographic studies (30 s *vs.* days), which rule out the fragmentation in capture experiments. Nevertheless, despite containing only a fragment of the molecule, the **fentanyl′@3′** structure allows us to get some insights into the host–guest interactions between the MOF and the part of the molecule within its pores, which might be also operative in the efficient capture of fentanyl molecules (see Table 1, S2† and Fig. 3) helping us to understand its exceptional effectiveness.

As similar adsorbates of the family, the crystal structure of **fentanyl′@3′** compound is isomorphous to **3** and crystallizes in the $P6_3$ chiral space group of the hexagonal system. Details of the structure (Fig. 6) show guest molecules statistically and

severely thermally disordered on three configuration sets (see Fig. S13 and S14†) residing in the pores. They represent the fragment of fentanyl molecules after a break on the 4-piperidinyl position, thus rejecting the piperidine moiety with the linked phenethyl group, and incorporating only the benzene ring and propionyl group connected to the central nitrogen atom.

They are packed *via* straight S···$N_{fentanyl'}$ and S···C=$O_{fentanyl'}$ bonds involving methionine residues [S···N and S···C=$O_{Centroid}$ distances of 1.84(1) and 2.20(1) Å], which block guest moieties embracing both kind of *arms*, in a *lock and key* fashion (Fig. 6c). Indeed, the pores are decorated with methionine residues exhibiting a distended conformation (Fig. 6a). Both S···$N_{fentanyl'}$ and S···C=$O_{fentanyl'}$ distances fall in the range of typical bonds. It is quite surprising, but it is worth considering **3′** as a nanoreactor. A fentanyl degradation occurs followed by a coordination reaction within pores. Such a situation has been observed in this family of MOFs[35] and, again, it might be ascribed to the extraordinary flexibility confined only in pores, for MOF **3**, where highly bendable arms are intrinsically prone to adopt different conformations of the thioether chains, depending on the different chemical environments determined by the guests' nature. In particular, the crystal structure of **fentanyl′@3′** shows methionine arms to be more distended than methyl-cysteine ones in **amphetamine@2′** and methionine in **amphetamine@3** (Fig. 4a and b), featuring available sulphur groups for interaction or even chemical bonds with electron donors – including oxygen and nitrogen atoms. Thus, they encapsulate the targeted guest molecules assuming the favourite conformation and interactions or bonds, in each case, to maximize their receptor assets. Indeed, **3** exhibits a quite unique dynamism and flexibility. It is the one related to the different conformations thioalkyl residues pointing toward the hexagonal channels adopt depending on the nature of the molecules hosted within its channels. These nice molecular recognition properties, together with the high crystallinity of **3**, allow us to have beautiful snapshots of the methionine residue conformations, which are shown in Fig. S15†. Overall, after analysing the presented crystal structures, we can conclude that the specific sulphur-based chemical functionalities pointing into the pores of our MOFs play a crucial role in dictating the observed interactions, particularly in relation to the molecular structures of amphetamine and fentanyl. So, our crystallographic analysis provides key insights into how these host–guest interactions govern the capture of such substances, which is instrumental in designing future porous materials with optimized adsorptive properties.

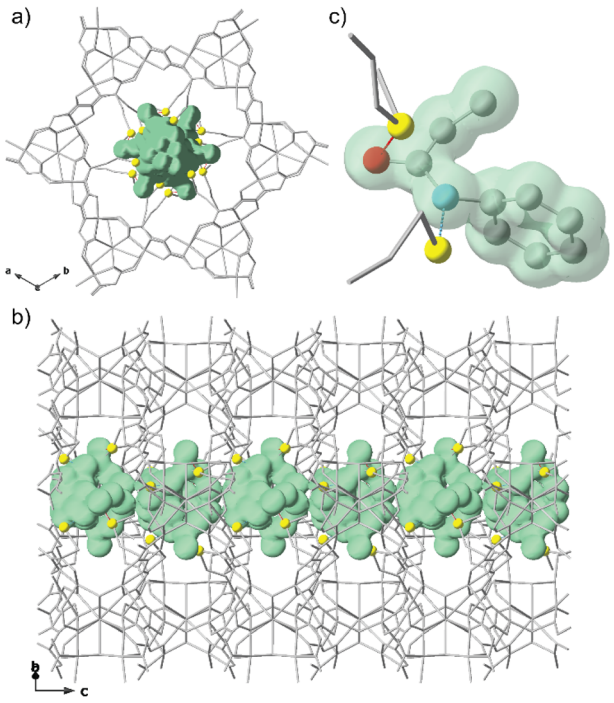

Fig. 6 Crystal structure of the host–guest aggregate **fentanyl′@3′** along the *c* (a) and *b* (b) axes. (c) Structure of the fragment of the fentanyl molecule emphasizing the host–guest interactions with sulphur atoms. Metals and organic ligands, with the exception of sulphur atoms (yellow spheres), constituting the network are represented with grey sticks. Green surfaces are used to emphasize the guest amphetamine molecules. Colour code: grey: carbon atoms; red: oxygen atoms; blue: nitrogen atoms.

In order to confirm the purity of the bulk samples of **amphetamine@2′**, **amphetamine@3** and **fentanyl′@3′**, powder X-ray diffraction (PXRD) studies were carried out for polycrystalline samples of these compounds, which confirm both that they maintain their structural integrity and also that all crystals are identical to those selected for SCXRD (Fig. S16–S18†). Moreover, aiming at verifying the robustness of MOF **3**, PXRD studies were carried out before and after the 16 reusability experiments (Fig. S19†), confirming that the material remains crystalline and unaltered after these experiments. Moreover, no leaching of metal atoms was observed after reusability experiments (as verified with ICM-MS experiments), which is not surprising considering that the robustness of these MOFs had been already confirmed.[38] Finally, the solvent contents were ultimately established with the help of thermogravimetric analyses (Fig. S20†).

3. Conclusions

Pollution of aquatic environments with emerging contaminants, such as drugs of abuse, poses risks to ecosystems and human health. These substances can disrupt aquatic life and potentially enter drinking water sources, raising concerns about their effects on both wildlife and humans. Addressing this issue is vital for protecting biodiversity and ensuring safe water. In this study, we present our findings on the use of a family of isoreticular MOFs, derived from amino acids, as solid-phase extraction (SPE) sorbents for the removal of a mixture of twenty-nine distinct recreational and medical drugs from aqueous solutions. Overall, all six materials demonstrate remarkable removal efficiency, with rapid adsorption kinetics (approximately 30 seconds) for the studied drug mixture. Notably, one of the MOFs exhibits exceptional capture efficiency for the simultaneous removal of all drugs in this mixture. This study also focuses on the removal efficiency and reusability of

fentanyl, a drug of particular concern, where MOF **3** shows outstanding performance and reusability, surpassing the current benchmark material (PAC). Finally, these remarkable and unexpected results have been rationalized with the insightful analysis of single-crystal X-ray diffraction of the host–guest adsorbates **amphetamine@2′**, **amphetamine@3** and **fentanyl′@3′**. This analysis suggests that the observed efficiency is attributed to the presence of appropriate functional groups decorating the MOF channels serving as selective receptors for this class of target molecules. The complete and simultaneous removal of contaminants of diverse nature poses a significant challenge and underscores the importance of the results presented here, representing a step forward in the design of new materials that can compete with traditional adsorbents like activated carbons,[61] zeolites[62] or porous materials with encapsulated metal nanoparticles[63] and be effectively implemented in real aquatic environments.

Data availability

The data supporting this article have been included as part of the ESI.†

Conflicts of interest

There are no conflicts of interest to declare.

Acknowledgements

This work was supported by the projects PID2021-125459OB-I00 and PID2022-136349OB-I00 funded by MCIN/AEI/10.13039/501100011033 and by "ERDF A way of making Europe", by the European Union, Excellence Unit "Maria de Maeztu" CEX2024-001467-M), and by the Ministero dell'Istruzione, dell'Università e della Ricerca (Italy). D. A. also acknowledges the financial support of the European Union – NextGenerationEU under the National Recovery and Resilience Plan (NRRP) of Ministero dell'Università e della Ricerca (MUR) (Project code PE0000021, "Network 4 Energy Sustainable Transition – NEST). Thanks are also extended to the "Generalitat Valenciana" (Project PROMETEO/2021/054). E. P. acknowledges the financial support of the European Research Council under the European Union's Horizon 2020 research and innovation programme/ERC Grant Agreement No. 814804, MOF-reactors. Thanks are also extended to the Ramón y Cajal Program, RYC2019-027940-I (J. F.-S.). This study forms part of the Advanced Materials programme (MFA/2022/048) and was supported by MCIN with funding from European Union NextGenerationEU (PRTR-C17.I1) and by Generalitat Valenciana.

Notes and references

1 T. W. Lo, J. W. K. Yeung and C. H. L. Tam, *Int. J. Environ. Res. Publ. Health*, 2020, **17**, 2610.
2 M. R. Boleda, M. T. Galceran and F. Ventura, *Water Res.*, 2009, **43**, 1126–1136.
3 B. Kasprzyk-Hordern, *Chem. Soc. Rev.*, 2010, **39**, 4466.
4 C. G. Daughton, *Rev. Environ. Contam. Toxicol.*, 2011, **210**, 59–110.
5 A. Rodayan, S. Afana, P. A. Segura, T. Sultana, C. D. Metcalfe and V. Yargeau, *Environ. Toxicol. Chem.*, 2016, **35**, 843–849.
6 G. Maasz, E. Molnar, M. Mayer, M. Kuzma, P. Takács, Z. Zrinyi, Z. Pirger and T. Kiss, *Environ. Toxicol. Chem.*, 2021, **40**, 1491–1498.
7 C. S. Skaggs and B. A. Logue, *Environ. Toxicol. Chem.*, 2022, **41**, 2658–2666.
8 T. Brodin, J. Fick, M. Jonsson and J. Klaminder, *Science*, 2013, **339**, 814–815.
9 L. Muñiz-Bustamante, N. Caballero-Casero and S. Rubio, *Environ. Int.*, 2022, **164**, 107281.
10 L. Belzak and J. Halverson, *Heal. Promot. Chronic Dis. Prev. Canada*, 2018, **38**, 224–233.
11 K. Kuczyńska, P. Grzonkowski, Ł. Kacprzak and J. B. Zawilska, *Forensic Sci. Int.*, 2018, **289**, 207–214.
12 S. Castiglioni, R. Bagnati, R. Fanelli, F. Pomati, D. Calamari and E. Zuccato, *Environ. Sci. Technol.*, 2006, **40**, 357–363.
13 C. Postigo, M. J. López de Alda and D. Barceló, *Environ. Int.*, 2010, **36**, 75–84.
14 T. L. Jones-Lepp, C. Sanchez, D. A. Alvarez, D. C. Wilson and R.-L. Taniguchi-Fu, *Sci. Total Environ.*, 2012, **430**, 237–245.
15 P. W. Seo, B. N. Bhadra, I. Ahmed, N. A. Khan and S. H. Jhung, *Sci. Rep.*, 2016, **6**, 34462.
16 A. Alsbaiee, B. J. Smith, L. Xiao, Y. Ling, D. E. Helbling and W. R. Dichtel, *Nature*, 2016, **529**, 190–194.
17 S. Lin, Y. Zhao and Y.-S. Yun, *ACS Appl. Mater. Interfaces*, 2018, **10**, 28076–28085.
18 D. Bradshaw, J. B. Claridge, E. J. Cussen, T. J. Prior and M. J. Rosseinsky, *Acc. Chem. Res.*, 2005, **38**, 273–282.
19 S. Kitagawa and R. Matsuda, *Coord. Chem. Rev.*, 2007, **251**, 2490–2509.
20 G. Férey, *Chem. Soc. Rev.*, 2008, **37**, 191–214.
21 J. R. Long and O. M. Yaghi, *Chem. Soc. Rev.*, 2009, **38**, 1213–1214.
22 T. Grancha, J. Ferrando-Soria, H.-C. Zhou, J. Gascon, B. Seoane, J. Pasán, O. Fabelo, M. Julve and E. Pardo, *Angew. Chem., Int. Ed.*, 2015, **54**, 6521–6525.
23 Y. Wen, P. Zhang, V. K. Sharma, X. Ma and H.-C. Zhou, *Cell Rep. Phys. Sci.*, 2021, **2**, 100348.
24 Q. Gao, J. Xu and X.-H. Bu, *Coord. Chem. Rev.*, 2019, **378**, 17–31.
25 S. Rojas and P. Horcajada, *Chem. Rev.*, 2020, **120**, 8378–8415.
26 D. Jiang, M. Chen, H. Wang, G. Zeng, D. Huang, M. Cheng, Y. Liu, W. Xue and Z. Wang, *Coord. Chem. Rev.*, 2019, **380**, 471–483.
27 M. Mon, R. Bruno, J. Ferrando-Soria, D. Armentano and E. Pardo, *J. Mater. Chem. A*, 2018, **6**, 4912–4947.
28 A. J. Howarth, Y. Liu, J. T. Hupp and O. K. Farha, *CrystEngComm*, 2015, **17**, 7245–7253.
29 C. Negro, P. Escamilla, R. Bruno, J. Ferrando-Soria, D. Armentano and E. Pardo, *Chem.–Eur. J.*, 2022, **28**, e202200034.
30 C. Negro, H. Martínez Pérez-Cejuela, E. F. Simó-Alfonso, J. M. Herrero-Martínez, R. Bruno, D. Armentano,

J. Ferrando-Soria and E. Pardo, *ACS Appl. Mater. Interfaces*, 2021, **13**, 28424–28432.
31 C. Negro, H. Martínez Pérez-Cejuela, E. F. Simó-Alfonso, W. Iqbal, J. M. Herrero-Martínez, D. Armentano, J. Ferrando-Soria and E. Pardo, *ACS Appl. Mater. Interfaces*, 2023, **15**, 3069–3076.
32 Y. Inokuma, M. Kawano and M. Fujita, *Nat. Chem.*, 2011, **3**, 349–358.
33 W. M. Bloch, N. R. Champness and C. J. Doonan, *Angew. Chem., Int. Ed.*, 2015, **54**, 12860–12867.
34 R. J. Young, M. T. Huxley, E. Pardo, N. R. Champness, C. J. Sumby and C. J. Doonan, *Chem. Sci.*, 2020, **11**, 4031–4050.
35 M. Viciano-Chumillas, M. Mon, J. Ferrando-Soria, A. Corma, A. Leyva-Pérez, D. Armentano and E. Pardo, *Acc. Chem. Res.*, 2020, **53**, 520–531.
36 K. Hyjek, G. Kurowski, K. Dymek, A. Boguszewska-Czubara, B. Budzyńska, O. Wronikowska-Denysiuk, A. Gajda, W. Piskorz, P. Śliwa, M. Szumera, P. Jeleń, M. Sitarz and P. J. Jodłowski, *Chem. Eng. J.*, 2024, **479**, 147655.
37 T. Baheri, Y. Yamini, M. Shamsayei and M. Tabibpour, *J. Sep. Sci.*, 2021, **44**, 2814–2823.
38 T. Grancha, J. Ferrando-Soria, J. Cano, P. Amorós, B. Seoane, J. Gascon, M. Bazaga-García, E. R. Losilla, A. Cabeza, D. Armentano and E. Pardo, *Chem. Mater.*, 2016, **28**, 4608–4615.
39 M. Baratta, T. F. Mastropietro, R. Bruno, A. Tursi, C. Negro, J. Ferrando-Soria, A. I. Mashin, A. Nezhdanov, F. P. Nicoletta, G. De Filpo, E. Pardo and D. Armentano, *ACS Appl. Nano Mater.*, 2022, **5**, 5223–5233.
40 R. Bruno, M. Mon, P. Escamilla, J. Ferrando-Soria, E. Esposito, A. Fuoco, M. Monteleone, J. C. Jansen, R. Elliani, A. Tagarelli, D. Armentano and E. Pardo, *Adv. Funct. Mater.*, 2021, **31**, 2008499.
41 A. Tursi, T. F. Mastropietro, R. Bruno, M. Baratta, J. Ferrando-Soria, A. I. Mashin, F. P. Nicoletta, E. Pardo, G. De Filpo and D. Armentano, *Adv. Mater. Interfaces*, 2021, **8**, 2100730.
42 M. Mon, F. Lloret, J. Ferrando-Soria, C. Martí-Gastaldo, D. Armentano and E. Pardo, *Angew. Chem., Int. Ed.*, 2016, **55**, 11167–11172.
43 H. M. Pérez-Cejuela, M. Mon, J. Ferrando-Soria, E. Pardo, D. Armentano, E. F. Simó-Alfonso and J. M. Herrero-Martínez, *Microchim. Acta*, 2020, **187**, 201.
44 M. Mon, R. Bruno, E. Tiburcio, M. Viciano-Chumillas, L. H. G. Kalinke, J. Ferrando-Soria, D. Armentano and E. Pardo, *J. Am. Chem. Soc.*, 2019, **141**, 13601–13609.
45 M. Mon, R. Bruno, E. Tiburcio, P.-E. Casteran, J. Ferrando-Soria, D. Armentano and E. Pardo, *Chem.–Eur. J.*, 2018, **24**, 17712–17718.
46 M. Mon, R. Bruno, J. Ferrando-Soria, L. Bartella, L. Di Donna, M. Talia, R. Lappano, M. Maggiolini, D. Armentano and E. Pardo, *Mater. Horiz.*, 2018, **5**, 683–690.
47 M. Mon, J. Ferrando-Soria, T. Grancha, F. R. Fortea-Pérez, J. Gascon, A. Leyva-Pérez, D. Armentano and E. Pardo, *J. Am. Chem. Soc.*, 2016, **138**, 7864–7867.
48 X. Kong, H. Deng, F. Yan, J. Kim, J. A. Swisher, B. Smit, O. M. Yaghi and J. A. Reimer, *Science*, 2013, **341**, 882–885.
49 H. Deng, C. J. Doonan, H. Furukawa, R. B. Ferreira, J. Towne, C. B. Knobler, B. Wang and O. M. Yaghi, *Science*, 2010, **327**, 846–850.
50 M. Viciano-Chumillas, X. Liu, A. Leyva-Pérez, D. Armentano, J. Ferrando-Soria and E. Pardo, *Coord. Chem. Rev.*, 2022, **451**, 214273.
51 J. Navarro-Alapont, C. Negro, S. Navalón, A. Dhakshinamoorthy, D. Armentano, J. Ferrando-Soria and E. Pardo, *Inorg. Chem.*, 2024, **63**, 13681–13688.
52 J. Rouquerolt, D. Avnir, C. W. Fairbridge, D. H. Everett, J. H. Haynes, N. Pernicone, J. D. F. Ramsay, K. S. W. Sing and K. K. Unger, *Pure Appl. Chem.*, 1994, **66**, 1739–1758.
53 L. S. Cheng and Y. Ralph T, *Chem. Eng. Sci.*, 1994, **49**, 2599–2609.
54 Y. Yan, E. J. Carrington, R. Pétuya, G. F. S. Whitehead, A. Verma, R. K. Hylton, C. C. Tang, N. G. Berry, G. R. Darling, M. S. Dyer, D. Antypov, A. P. Katsoulidis and M. J. Rosseinsky, *J. Am. Chem. Soc.*, 2020, **142**, 14903–14913.
55 A. Tartaglia, M. Locatelli, A. Kabir, K. G. Furton, D. Macerola, E. Sperandio, S. Piccolantonio, H. I. Ulusoy, F. Maroni, P. Bruni, F. Croce and V. F. Samanidou, *Molecules*, 2019, **24**, 382.
56 E. Tiburcio, R. Greco, M. Mon, J. Ballesteros-Soberanas, J. Ferrando-Soria, M. López-Haro, J. C. Hernández-Garrido, J. Oliver-Meseguer, C. Marini, M. Boronat, D. Armentano, A. Leyva-Pérez and E. Pardo, *J. Am. Chem. Soc.*, 2021, **143**, 2581–2592.
57 W. B. Motherwell, R. B. Moreno, I. Pavlakos, J. R. T. Arendorf, T. Arif, G. J. Tizzard, S. J. Coles and A. E. Aliev, *Angew. Chem., Int. Ed.*, 2018, **57**, 1193–1198.
58 M. Schackmuth and S. Kerrigan, *J. Forensic Sci.*, 2024, **69**, 1799–1814.
59 M. Mon, R. Bruno, S. Sanz-Navarro, C. Negro, J. Ferrando-Soria, L. Bartella, L. Di Donna, M. Prejanò, T. Marino, A. Leyva-Pérez, D. Armentano and E. Pardo, *Nat. Commun.*, 2020, **11**, 3080.
60 P. Escamilla, L. Bartella, S. Sanz-Navarro, R. M. Percoco, L. Di Donna, M. Prejanò, T. Marino, J. Ferrando-Soria, D. Armentano, A. Leyva-Pérez and E. Pardo, *Chem.–Eur. J.*, 2023, **29**, e202301325.
61 M. Jaya Rajan and C. Indira Anish, in *Water Quality - New Perspectives*, IntechOpen, 2024.
62 T. Bajda, A. Grela, J. Pamuła, J. Kuc, A. Klimek, J. Matusik, W. Franus, S. K. K. Alagarsamy, T. Danek and P. Gara, *Materials*, 2024, **17**, 3848.
63 J. Mangalam, J. Sharma, M. Sharma, Y. K. Mishra, S. Nigam and M. Joshi, *Clean Technol. Environ. Policy*, 2024, **26**, 1705–1729.

